Werk

Jahr: 1977
Kollektion: fid.geo
Signatur: 8 Z NAT 2148:44
Digitalisiert: Niedersächsische Staats- und Universitätsbibliothek Göttingen
Werk Id: PPN1015067948_0044
PURL: http://resolver.sub.uni-goettingen.de/purl?PPN1015067948_0044

LOG Id: LOG_0022
LOG Titel: Plasma measurement during the Western Euopean winteranomaly campaign
LOG Typ: article

Übergeordnetes Werk

Werk Id: PPN1015067948
PURL: http://resolver.sub.uni-goettingen.de/purl?PPN1015067948
OPAC: http://opac.sub.uni-goettingen.de/DB=1/PPN?PPN=1015067948

Contact

Niedersächsische Staats- und Universitätsbibliothek Göttingen
Georg-August-Universität Göttingen
Platz der Göttinger Sieben 1
37073 Göttingen
Germany
Email: gdz@sub.uni-goettingen.de

J. Geophys. 44, 81–90, 1977

Journal of Geophysics

Plasma Measurements during the Western European Winteranomaly Campaign

K. Spenner, W. Ott, and H.J. Bradenstein
Institut für Physikalische Weltraumforschung der FhG,
D-7800 Freiburg, Federal Republic of Germany

Abstract. During theWestern European Winteranomaly Campaign two planar Retarding Potential Analyzers were successfully launched on January 4 and 21, 1976 from El Arenosillo, Spain. The experiment on board the B II payload which carried two sensor heads is described. The payload had an active attitude control system with Freon gas as propellent. Its influence upon the plasma measurements is investigated. In the height range 95 to 115 km measured profiles of electron density, temperature and suprathermal electron flux are presented.

Key words. Retarding potential analyzer – Winteranomaly – Electron density – Electron temperature – Suprathermal electron flux – Disturbances by attitude control system.

Introduction

The Western European Sounding Rocket Campaign took place in January 1976 at "El Arenosillo", Spain (37°6′N, 6°44′W) with a large number of different measurements. The scientific purpose of this combined effort of ground based and rocket carried experiments was to investigate the ionospheric D-region during a winteranomaly. A typical indicator for a winteranomaly condition is unusually great radio wave absorption during a couple of days in a large geographic area. The phenomenon is supposed to be caused by increased electron density in the lower ionosphere through the regular seasonal variation of the state of mesosphere and lower thermosphere (Schwentek, 1971). The not well known relations between ionospheric plasma parameters and neutral composition, and the rather complex processes involved in the D-region can only be studied in more detail when a large number of significant parameters are simultaneously measured. As a part of such a combined study two Retarding Potential Analyzers (RPA) were successfully flown aboard a Skylark rocket in the afternoon of January 4 and 21, 1976. The main thermal plasma parameters viz

electron density and temperature, and the suprathermal electron flux were derived from the measured characteristics. The electron density profile shows the altitude, where the anomaly occurs and how strong it is. Electron temperature and flux may be influenced by the neutral atmosphere and could respond to major changes in the neutral composition.

Instrumentation

We used a planar RPA, similar to an instrument which was flown on earlier rockets and satellites (Spenner et al., 1974). The sensor has a wide entrance grid and a small collector plate as shown in Figure 1. The large first grid and the guard ring surrounding the collector provide for radially uniform particle flux about the sensor axis. The collector samples only electrons or ions from this uniform central region. The sensor has 5 insulated, highly transparent grids. With suitable potentials of these any desired kind of charged particles may be selected and analyzed. In the electron mode the front grids G1, G2, G3 are connected and obtain a staircase retarding voltage; with three grids a most uniform retarding field is achieved. Only electrons with a higher energy than the applied grid voltage can pass through to the collector. Grids G4 and G5 are biased in such a way that ambient ions and secondary electrons produced at the collector are almost completely suppressed. The gold plated grids have 30 wires/cm, the transparency is 86%.

The experiment automatically performs three different modes. Electron temperature and relative density are derived from a 'temperature mode', the suprathermal energy distribution from a 'photoelectron mode' and the ion density from an 'ion mode'. Table 1 summarizes the voltages applied to the sensor grids for the different modes. Each electron mode makes a sequence of 128 steps of 40 mV each. The photoelectron mode executes 28 steps of 1.1 V each. The stepping time is 2 ms. We use a RPA with two identical sensor heads fastened on short booms at the top of the payload (Fig. 2). One sensor is programmed to measure electron temperature and photoelectrons, the other one to determine the ion density with good local resolution. A logarithmic electrometer integrated in the sensor box measures the collector current between the limits 10^{-5} A and 10^{-12} A. Zero level and gain are automatically controlled

Table 1

Symbol	Element	Temperature Mode	Ion density Mode	Photoelectron Mode
G 1	Entrance grid	3→ −1.5	0	4
G 2	Retarding grid 1	3→ −1.5	−6.2	0→ −30
G 3	Retarding grid 2	3→ −1.5	−6.2	0→ −30
G 4	Shielding grid	30	0	30
G 5	Electron suppressor grid	15	−15	15
C, CR	Collector, Guardring	30	0	30

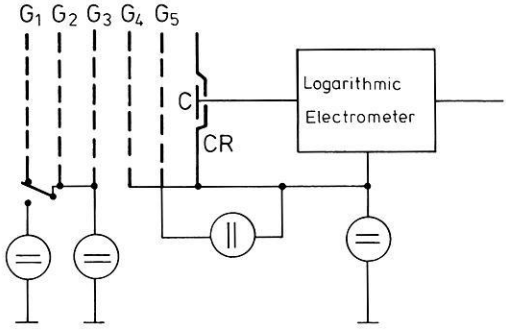

Fig. 1. Sensor schematic of the RPA

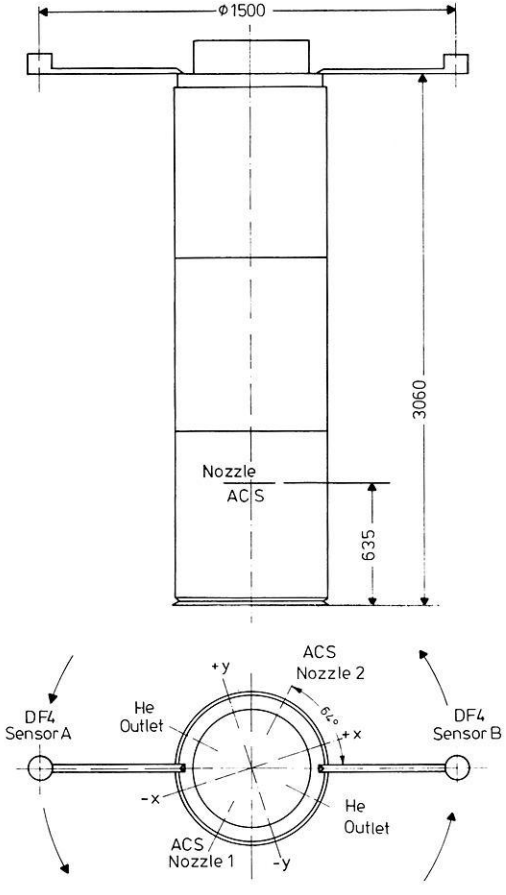

Fig. 2. Position of the RPA and the gas nozzles of the ACS

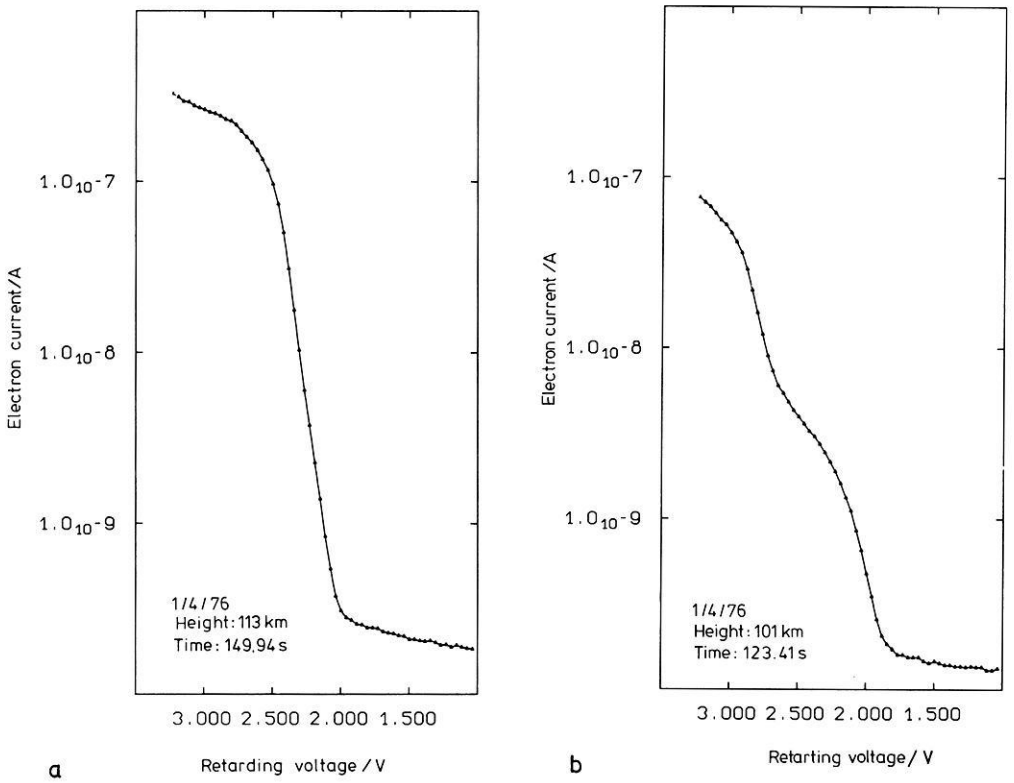

Fig. 3. a Measured Langmuir characteristic showing a Maxwellian energy distribution of the thermal electrons. **b** Langmuir characteristic of negative particles with two different energy distributions

and adjusted. Includig the bit failure of the 10 bit telemetry the overall accuracy is about 2%. For currents larger than 10^{-11} A the electrometer rise time (99%) is 2 ms. The additional electronics needed to provide the sensor grid voltages, as well as power supply and telemetry interface are installed in a separate box. The achieved stability of the retarding voltages is 0.5 mV. Design and calibration of the instrument are such that electron density and temperature can be measured with an accuracy better than 10%.

Because of the needs of the mass spectrometer the B II payload had an active attitude control system (ACS) so as to point the rocket axis always in the direction of the velocity vector. Thus, the RPA axis was always oriented to optimum ram direction, during ascent and descent. The payload control was achieved by a pulsed Freon gas beam, which was fired about once a spin period (0.5 s). As a consequence the natural environment near the rocket was influenced by a Freon cloud. Its influence to the plasma measurements will be discussed in the following section. The position of the Freon outlets (Nozzle 1 and 2) relative to the RPA sensors is shown in Figure 2. In addition to this there was a Helium outlet of the cooling system of the cryomass-Spectrometer.

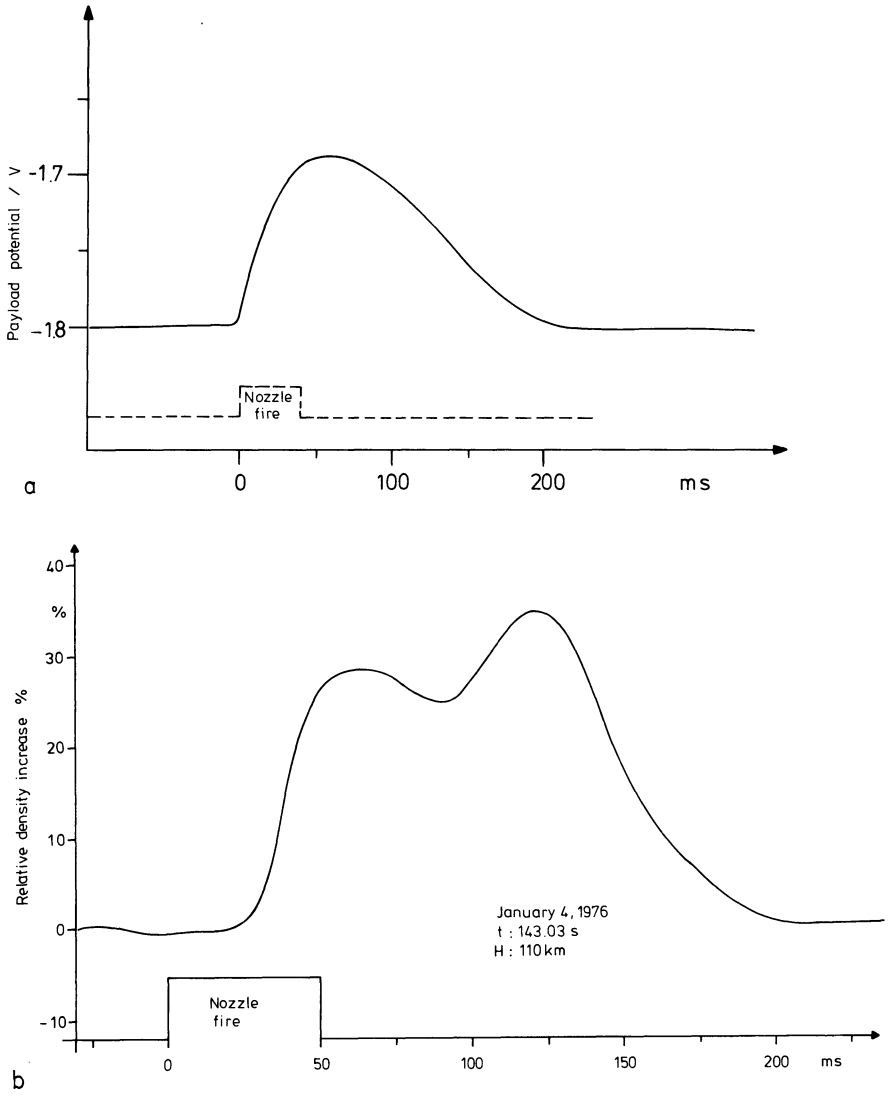

Fig. 4. a Time dependent potential variation of the payload after Freon gas release. **b** Relative plasma density increase after nozzle fire

Results

The transmitted RPA data are of excellent quality for both flights. After boom deployment at 90 km altitude the Langmuir current-voltage characteristic appeared at Sensor A and the ion saturation current at Sensor B. In Figure 3a an example of such a half-logarithmic current-voltage curve is shown. The most important part of the curve is linear with a decrease by about 2 orders of magnitude. Such curve is expected for a Maxwellian energy distribution of the electrons. The maximum slope of this curve determines the electron

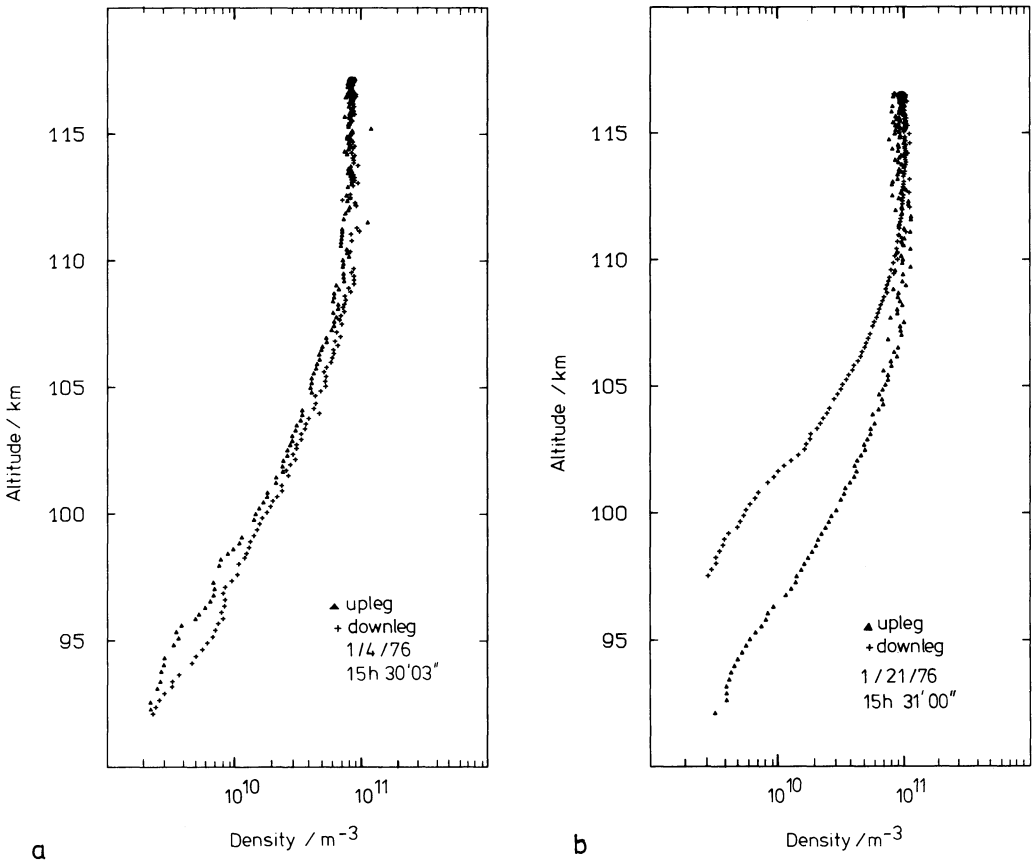

Fig. 5 a Electron density profile for January 4. **b** Electron density profile for January 21

temperature. All current-voltage curves were analyzed. During ascent we found at 100 km altitude an unexpected hump in the lower part of the characteristics as shown in Figure 3b. This proves that a second negative particle population is present with higher than thermal energy. The hump is increased after a nozzle fire. During descent no hump was observed in the same height region. This leads us to suppose that the observed particles are not of natural ionospheric origin. We assume that outgasing, may be in connection with the Freon release, produces negative ions. A rough analysis shows that the hypothesis of negative ions with a mass number greater than 50 mu and a temperature below 300 K is agreeable with the observed curve. At altitudes where these particles are present the true electron temperature can not be obtained by the usual automatic program such that individual analysis is needed.

During each nozzle firing of the ACS the payload is surrounded by a Freon cloud expanding into space. We try to point out how this gas release effects the thermal plasma measurements. The first serious effect is that the payload potential which uses to be always negative in the ionosphere becomes more positive. A corresponding voltage shift in the Langmuir curves is observed after every nozzle fire. The potential increase is between 120 and 200 mV.

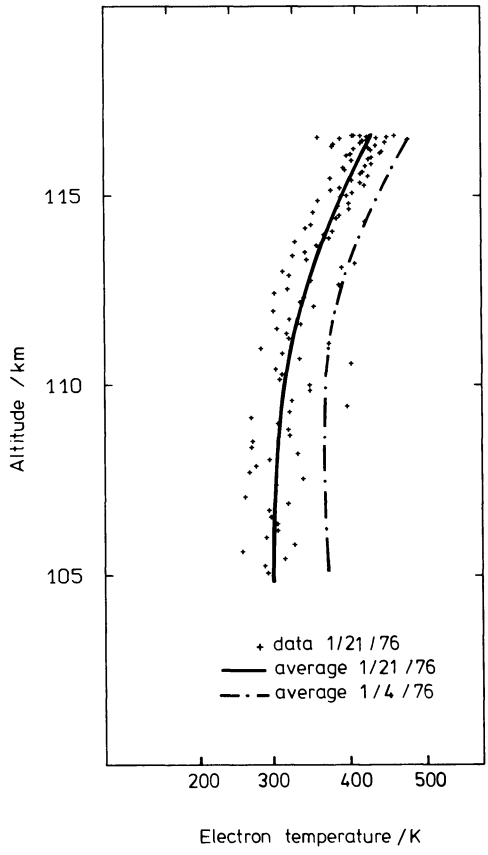

Fig. 6. Electron temperature profiles for January 4 and January 21

The time delay between the gas release and the potential change is probably less than 10 ms, which is the time resolution of the nozzle fire signal. Figure 4a shows the variation of the payload potential during firing of a nozzle (this is an observation of an earlier rocket flight with the same propellant gas). A short gas release leads to a potential change lasting about 200 ms. During that period the plasma density in the neighbourhood of the payload is changed and the ratio between the positive ion and the negative particle flux to the rocket is increased. Secondly we observe an increase of the measured ion current by up to 30% and more as shown in Figure 4b. A first current peak is observed between 20 and 70 ms after the nozzle fire followed by a more pronounced second peak. The observed minimum between the peaks is consistent with the assumption that the plasma density has a minimum at the side opposite to the firing nozzle due to the shadow of payload. This rarefied area is crossed by the spinning sensor B always 90 ms after a nozzle-1-fire (see Fig. 2). Within 200 ms the electron current measured by sensor A was also increased. This confirms that the plasma density is usually enlarged by ionization of the gas released from the ACS. For sensor B the density enhancement is more pronounced when the closer nozzle 2 is activated. The described effects are observed quite generally with only one exception namely at the apogee of the second

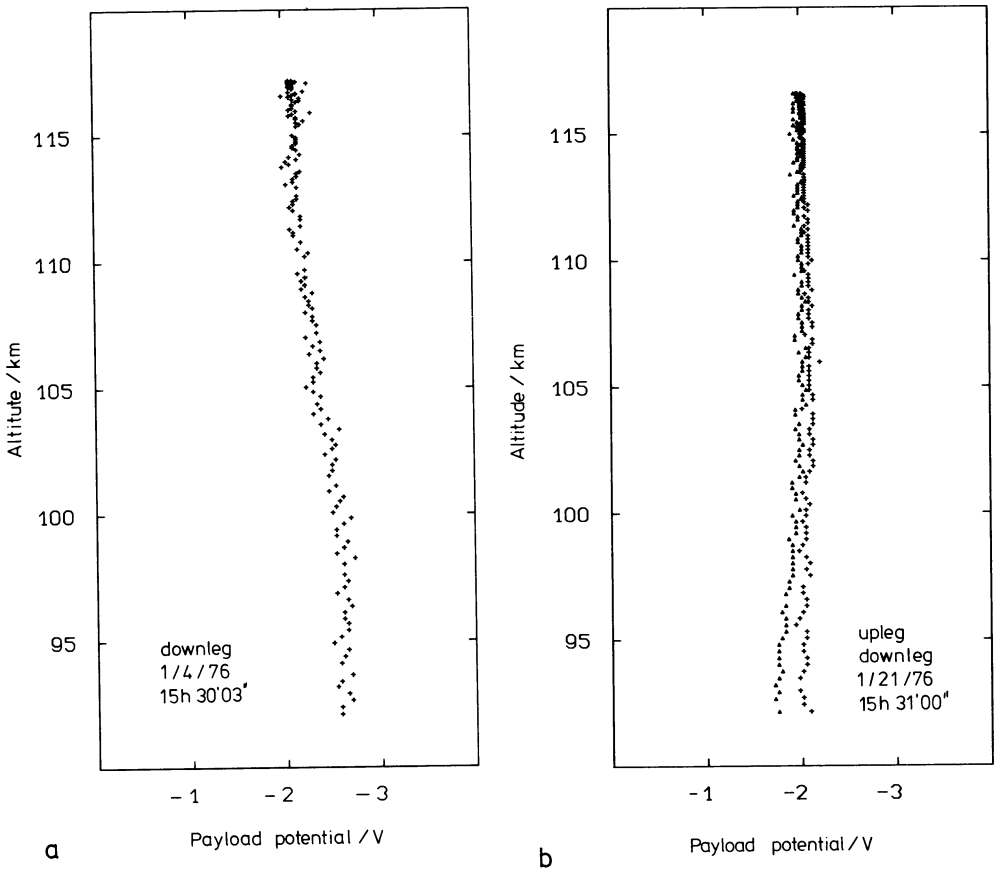

Fig. 7 a Payload potential for January 4. **b** Payload potential for January 21

flight. When there for about 10 s a large amount of gas was released the plasma density did not increase, but decreased.

We determined the ion density from the current of Sensor B according to the equation

$$n = \frac{I}{qFTv\cos\vartheta} \tag{1}$$

I is the current averaged over 0.3 s, F the effective area of the collector, q the elementary charge, T the grid transparency, v the rocket velocity and ϑ the angle between rocket velocity vector and sensor axis. Equation (1) is a good approximation for the saturation current as long as $v\cos\vartheta$ is much greater than the thermal ion velocity. This is true during the whole flight pass because the apogee velocity was greater than 800 ms^{-1}. The density profiles of both flights are shown in Figures 5a and b. (These data are not yet corrected for the density increase due to the ACS. Up and downleg of the January 4 density profile fit well together. As for January 21 the apparent discrepancy between

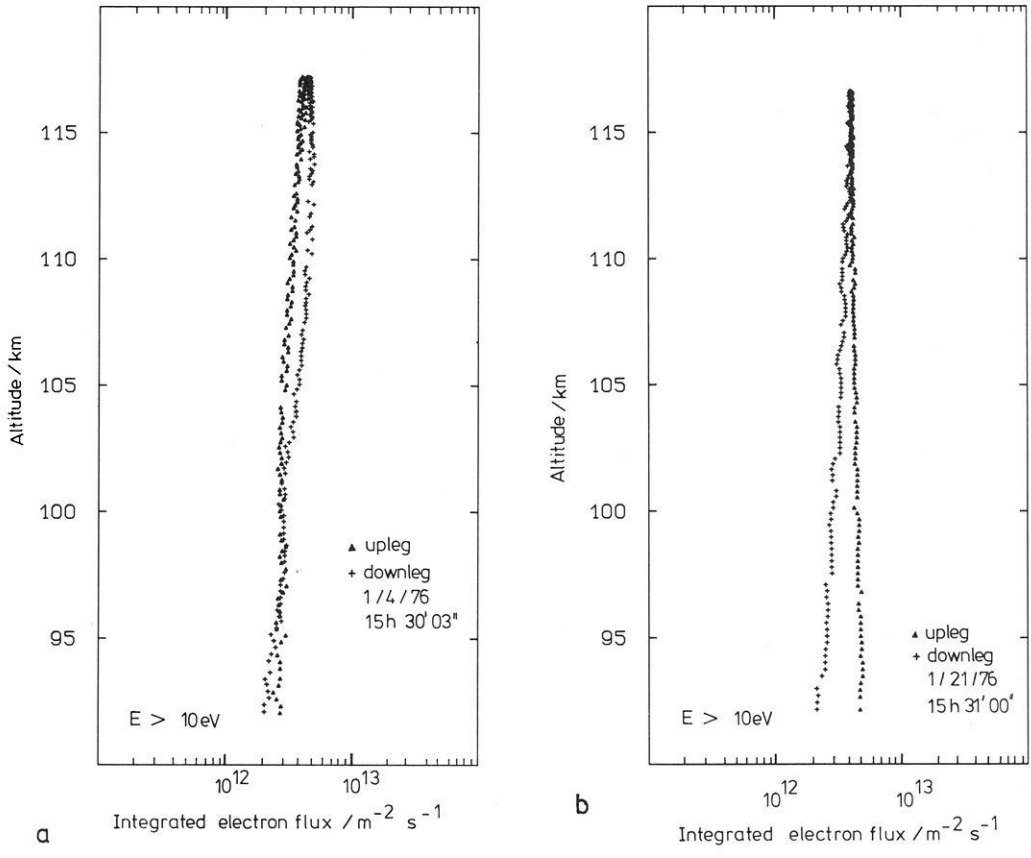

Fig. 8. a Integrated electron flux for January 4. **b** Integrated electron flux for January 21

ascent and descent could still be due to incorrect orbit calculation. Upleg and downleg profile can be matched together when the computed apogee height is reduced). Both profiles show a maximum density of $9 \cdot 10^{10}$ m^{-3}; there is no significant deviation from an expected E-region profile under daylight conditions.

Because of the earlier mentioned not Maxwellian Langmuir characteristic during ascent, we could readily deduce the electron temperature only with the downleg data. The density change and the potential shift caused by the ACS deform the slope of the current-voltage curves to higher and lower values depending on the time after nozzle fire. As a consequence we get some scatter between the individual data points and an averaged more significant temperature profile. Figure 6 shows the individual data points and the averaged temperature for January 21 and for the smoothed temperature profile of January 4, with clearly higher temperature.

The potential of the payload is determined from the highest slope of the semilogarithmic current-voltage curve. We get a rather negative charge as shown in Figures 7a and b. Compared with other rocket flights the rocket potential

of -2 V or more is quite important. This could be the result of the rather small ratio of the effective ion collecting area in ram position and the total surface of the payload (which collects the faster electrons).

In the last Figures 8a and b the integral electron flux above 10 eV is shown. The flux profile of the first flight has no significant difference between up and downleg, which indicates nearly isotropic flux. During the second flight the data show that the downcoming flux measured during ascent is higher and almost independent of the altitude. However, since we had attitude control with increasing height the sensor points more and more horizontaly so that a vertical flux which might grow slowly with height may not be recognized.

5. Conclusions

The data presented are not yet corrected for the disturbance caused by the gas release of the ACS and must therefore be considered as preliminary. The calculated height of the second flight may be in error by one or two km. All that, however, does not effect seriously the more general results. During these anomalous winter days in the height range 100–115 km we could not observe a significant deviation of the electron density profile from normal E-region behaviour. The strong radio wave absorption observed by ground based measurements is only due to a strong density enhancement in the D-region. The downward directed suprathermal electron flux was smaller for January 4. Assuming that the total production of photoelectrons was equal on both days (as it is measured for the upward flux) we may argue that the downward flux was more absorped on January 4. At the same time the electron temperature was increased. Now it is well known that the slowing-down process of photoelectrons depends on the neutral atmosphere. An increased atomic oxygen density, for example, on January 4 could absorb a larger amount of the photoelectrons produced at a higher altitude range. (Dalgarno et al., 1971). A part of the photelectron energy is always transferred to the thermal electrons. The increased electron temperature and atomic oxygen density as measured by the mass-spectrometer are in agreement with these considerations. A more complete picture may later be determined when the whole set of simultaneous measurements becomes available.

Acknowledgements. We thank the BMFT for sponsoring this project funded unter Kapitel 3006, titel 68501.

We appreciate the support we had from the DFVLR/BPT We wish to thank the project scientist of this Western European Winteranomaly Campaign, Prof. Offermann for great encouragement and fruitful cooperation.

References

Dalgarno, A., Lejeune, G.: The absorption of electrons in atomic oxygen, Planetary Space Sci. **19**, 1653–1667, 1971

Schwentek, H.: Regular and irregular behaviour of the winteranomaly in ionospheric absorption. J. Atmospheric Terrest. Phys. **33**, 1647–1650, 1971

Spenner, K., Dumbs, A.: The retarding potential analyzer on AEROS-B, J. Geophys. **40**, 585–592, 1974

Received May 2, 1977